A Framework for Multi-Planet Flyby Targeting

Goktug Bicak

Abstract

Sending spacecraft into deep space is heavily limited by Tsiolkovsky's rocket equation, which shows that fuel requirements scale exponentially with every extra bit of velocity change (Δv) needed for a mission. Planetary gravity assists bypass this limit by extracting a fraction of a planet's orbital momentum to alter a spacecraft's direction and speed without consuming propellant. This project constructed a patched-conic trajectory simulation tool in Python that integrates a universal-variable Lambert solver with a backwards-propagation algorithm to design and evaluate multi-planet transfers. Model accuracy was verified against published NASA mission data for Voyager 2 at Jupiter and Saturn and Cassini at Venus (Jet Propulsion Laboratory, 1979; Jet Propulsion Laboratory, 1998). Calculated values matched published periapsis distances within 0.42% and relative velocities within 0.35% (Jet Propulsion Laboratory, 1979; Jet Propulsion Laboratory, 1998). Applying this framework to an Earth–Venus–Earth–Saturn (EVES) multi-flyby mission demonstrates that the required launch velocity (Δv_launch) decreases from 15.72 km/s for a direct transfer to 8.24 km/s, though total travel time increases from 6.01 years to 7.80 years (Vallado, 2013; Jet Propulsion Laboratory, 1979; Jet Propulsion Laboratory, 1998).

1.0 Introduction

1.1 Project Motivation and Objectives

When planning missions to the outer solar system, sending a payload directly using chemical propulsion quickly becomes impractical. The primary constraint is governed by Tsiolkovsky's rocket equation (Bate et al., 1971; Curtis, 2020):

$$\Delta v = v_e \times \ln(m_0 / m_f) \quad \text{(Equation 1)}$$

where v_e represents effective exhaust velocity, m_0 is initial wet mass, and m_f is final dry mass (Bate et al., 1971; Curtis, 2020). Because mass ratios scale exponentially with higher velocity requirements, launching heavy payloads directly to outer planets such as Saturn demands launch vehicles far exceeding current technological capabilities.

While space agencies utilize high-fidelity N-body numerical simulations for final mission design, preliminary trajectory exploration requires a computationally efficient method to screen

thousands of potential launch windows. The objective of this project is to determine whether a simplified patched-conic framework employing Lambert targeting and backwards propagation can accurately model complex gravity assists and evaluate mission trade-offs without requiring full numerical integration.

It is hypothesized that a backwards-propagating patched-conic model can reproduce historical NASA flyby parameters within 1% error while enabling rapid parametric trade studies comparing launch energy against total travel time for multi-planet routes (Jet Propulsion Laboratory, 1979; Jet Propulsion Laboratory, 1998).

1.2 Historical Background

Gravity assists have served as a cornerstone of deep space exploration since the late 20th century (Bate et al., 1971; Jet Propulsion Laboratory, 1979). During the Voyager 2 mission launched in 1977, a rare geometric alignment of the outer planets enabled sequential flybys of Jupiter, Saturn, Uranus, and Neptune (Jet Propulsion Laboratory, 1979). The Jupiter encounter imparted sufficient heliocentric energy to accelerate the spacecraft toward Saturn in less than half the duration of a direct transfer (Jet Propulsion Laboratory, 1979). Similarly, the Cassini-Huygens mission launched in 1997 executed a complex Venus–Venus–Earth–Jupiter Gravity Assist (VVEJGA) trajectory to reach Saturn (Jet Propulsion Laboratory, 1998). By looping past Venus twice and performing a gravity assist at Earth, Cassini accumulated the necessary velocity incrementally over several years, enabling a heavy scientific payload to be launched on an existing launch vehicle (Jet Propulsion Laboratory, 1998).

2.0 Physics and Orbital Mechanics Background

2.1 Keplerian Orbital Elements

In a simplified two-body system, an orbit is uniquely defined by six Keplerian orbital elements (Bate et al., 1971; Curtis, 2020):

- Semi-major axis (a): Specifies the orbital size and total mechanical energy.
- Eccentricity (e): Defines the orbital shape (e = 0 for circular, 0 < e < 1 for elliptical, e > 1 for hyperbolic).
- Inclination (i): Measures the tilt relative to the reference ecliptic plane.
- Right Ascension of Ascending Node (Ω): Sets the angle where the orbit crosses upward through the reference plane.
- Argument of Periapsis (ω): Defines the orientation of periapsis from the ascending node.

- True Anomaly (v): Tracks the real-time angular position of the spacecraft along its trajectory (Bate et al., 1971; Curtis, 2020).

The specific mechanical energy ε depends solely on the semi-major axis a (Bate et al., 1971; Curtis, 2020):

$$\varepsilon = (v^2 / 2) - (\mu / r) = -\mu / (2a) \quad \text{(Equation 2)}$$

where $\mu = G \times M$ represents the gravitational parameter of the primary body ($\mu_{Sun} = 1.327 \times 10^{11}$ km³/s²), v is orbital speed, and r is radial distance (Bate et al., 1971; Curtis, 2020).

2.2 Hyperbolic Flyby Mechanics

During a planetary encounter, a spacecraft's trajectory within the planet's sphere of influence (SOI) forms a hyperbola (e > 1) (Curtis, 2020; Vallado, 2013). Relative to the planet, the incoming asymptotic speed $v_{\infty,in}$ equals the outgoing asymptotic speed $v_{\infty,out}$ (Curtis, 2020; Vallado, 2013):

$$v_\infty = ||v_{\infty,in}|| = ||v_{\infty,out}|| \quad \text{(Equation 3)}$$

Planetary gravity deflects the relative velocity vector through a turning angle δ (Curtis, 2020; Vallado, 2013):

$$\sin(\delta / 2) = 1 / [1 + (r_p \times v_\infty^2 / \mu_{planet})] = 1 / e \quad \text{(Equation 4)}$$

where r_p denotes the periapsis radius (Curtis, 2020; Vallado, 2013).

None
[Inbound Hyperbola: $v_{\infty,in}$] ———▶ (Periapsis r_p) ———▶ [Outbound Hyperbola: $v_{\infty,out}$]
|
[Deflection Angle δ]

Figure 1: Hyperbolic flyby trajectory geometry inside a planet's sphere of influence.

Even though relative speed remains constant during an unpowered flyby, vector rotation alters the spacecraft's heliocentric velocity (Curtis, 2020; Vallado, 2013):

$v_{hel,out} = v_{planet} + v_{\infty,out}$ (Equation 5)

$v_{hel,in} = v_{planet} + v_{\infty,in}$ (Equation 6)

$\Delta v_{hel} = v_{hel,out} - v_{hel,in} = v_{\infty,out} - v_{\infty,in}$ (Equation 7)

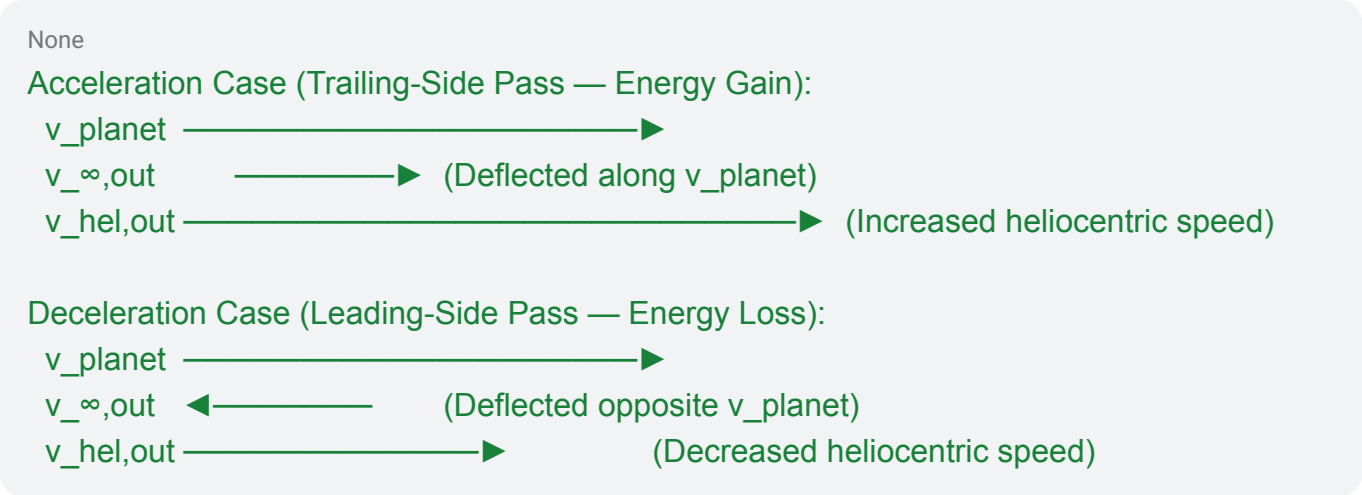


Figure 2: Vector addition illustrating heliocentric velocity gain and loss during a planetary flyby.

Figure 2 demonstrates how vector addition governs heliocentric velocity changes during a flyby (Curtis, 2020; Vallado, 2013). When the spacecraft passes behind the planet (trailing-side flyby), $v_{\infty,out}$ rotates more closely into alignment with the planet's orbital velocity vector (v_{planet}), increasing the magnitude of $v_{hel,out}$ and extracting orbital energy from the planet to boost the spacecraft into a higher solar orbit. Conversely, when the spacecraft passes ahead of the planet (leading-side flyby), $v_{\infty,out}$ is deflected opposite to v_{planet}, decreasing the magnitude of $v_{hel,out}$ so the spacecraft loses heliocentric energy and drops into a lower orbit around the Sun (Curtis, 2020; Vallado, 2013).

2.3 Physical Flyby Limits

To ensure physical realism, periapsis altitude h_p above the planetary surface is constrained (Vallado, 2013):

$r_p = R_{planet} + h_p$ (Equation 8)

Minimum altitude limits (h_min) are set to 300 km for terrestrial planets to clear atmospheric drag, and 50,000 km for gas giants to avoid planetary ring systems and intense radiation belts (Vallado, 2013; Jet Propulsion Laboratory, 1979; Jet Propulsion Laboratory, 1998).

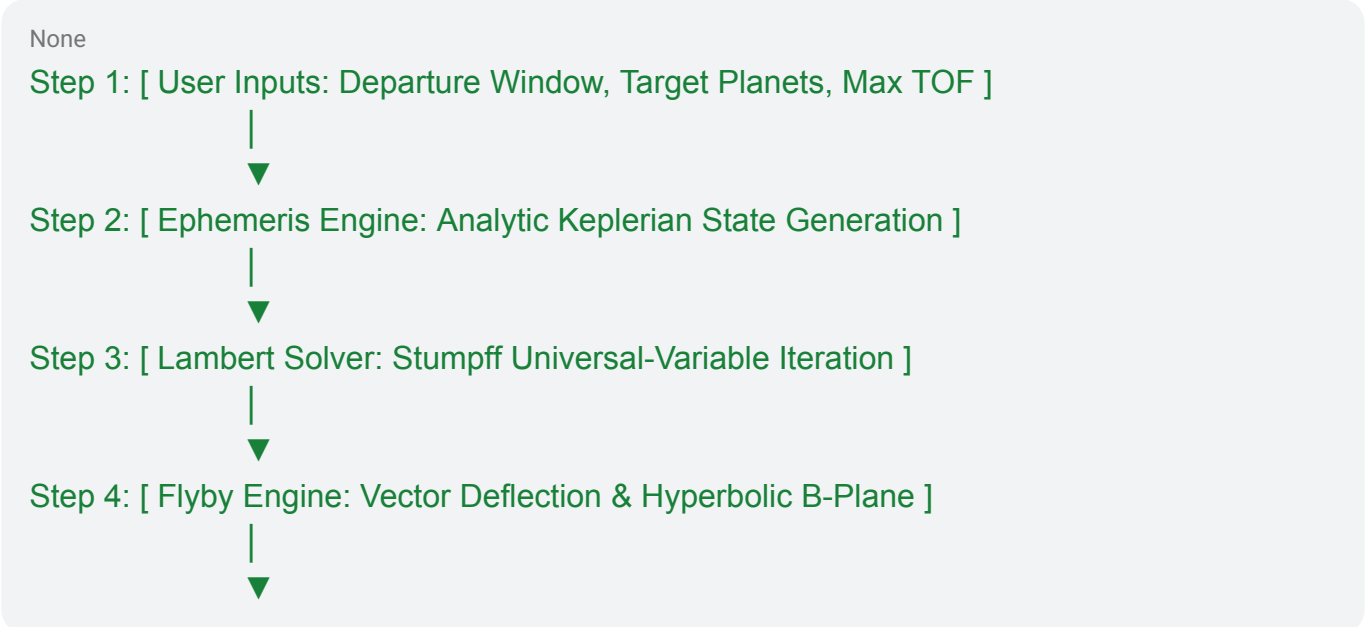
Table 1: Planetary constants and physical constraints used in calculations (Vallado, 2013; Jet Propulsion Laboratory, 1979).

Body	Gravitational Parameter μ (km^3/s^2)	Mean Radius R_planet (km)	Minimum Altitude h_min (km)
Venus	324,859	6,052	300
Earth	398,600	6,371	300
Jupiter	126,686,534	69,911	50,000
Saturn	37,931,187	58,232	50,000

3.0 Program Architecture & Methodology

3.1 Code Flow

The simulation software is structured into a modular processing pipeline implemented in Python:



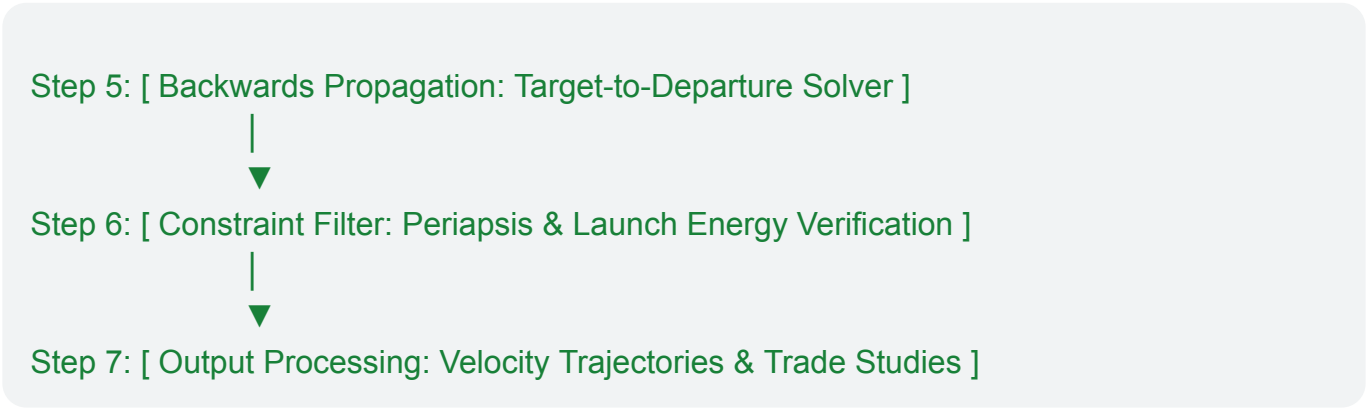


Figure 3: Program pipeline and execution workflow of the trajectory simulation code.

3.2 Patched Conic Modeling

The patched conic model is essential because full N-body differential numerical integration is computationally prohibitive when screening thousands of potential launch windows across multi-year mission designs. By decomposing complex gravitational fields into a sequence of two-body problems, the patched-conic approximation reduces computational overhead while maintaining high analytical fidelity (Curtis, 2020; Vallado, 2013).

Within this simulation, each transfer is segmented into three distinct dynamical phases:

1. Heliocentric Departure Arc: A Sun-centered elliptical transfer orbit from the departure planet to the target planet's Sphere of Influence (SOI) boundary (Curtis, 2020; Vallado, 2013).
2. Hyperbolic Planet Encounter: A planet-centered hyperbolic flyby within the planet's SOI, where the SOI radius r_SOI is determined by Laplace's formula (Curtis, 2020; Vallado, 2013):

$$r_{SOI} = a_p \times (m_p / M_{Sun})^{(2/5)} \quad \text{(Equation 9)}$$

3. Heliocentric Outbound Arc: A subsequent Sun-centered elliptical trajectory from the flyby planet onward to the next destination or final target (Curtis, 2020; Vallado, 2013).

3.3 Universal Variable Lambert Solver

Given an initial position vector r_1, final position vector r_2, and target time of flight (TOF = t_2 - t_1), Lambert's problem solves for the required terminal velocity vectors v_1 and v_2 (Curtis,

2020; Vallado, 2013). To robustly handle elliptical, parabolic, and hyperbolic transfer orbits without numerical singularities, the solver is formulated using universal variables and Stumpff functions C(z) and S(z), where $z = \alpha \times y^2$ (Curtis, 2020; Vallado, 2013):

$C(z) = (1 - \cos(\sqrt{z})) / z \quad (\text{for } z > 0) \quad (\text{Equation 10})$

$S(z) = (\sqrt{z} - \sin(\sqrt{z})) / (\sqrt{z})^3 \quad (\text{for } z > 0) \quad (\text{Equation 11})$

Stumpff functions C(z) and S(z) are evaluated directly inside a Newton-Raphson iteration loop to solve Kepler's universal time-of-flight equation for the universal variable z. Physically, z is a dimensionless parameter representing scaled orbital energy ($z = \alpha \times y^2$, where $\alpha = 1/a$ is the reciprocal of the transfer semi-major axis and y is the universal anomaly). Once the solver converges on z, C(z) and S(z) are used to compute the Lagrange coefficients f, g, and g_dot, which yield the terminal velocity vectors (Curtis, 2020; Vallado, 2013):

$v_1 = (r_2 - f \times r_1) / g \quad (\text{Equation 12})$

$v_2 = (g_dot \times r_2 - r_1) / g \quad (\text{Equation 13})$

These terminal velocities are required because v_1 defines the spacecraft's exact heliocentric departure velocity needed to leave the first planet on an intercept course, while v_2 defines its arrival velocity at the next planet, which determines the incoming excess speed ($v_{\infty,in}$) available for the subsequent gravity assist (Curtis, 2020; Vallado, 2013).

3.4 Backwards-Propagation Targeting

Forward propagation of multi-leg trajectories accumulates small numerical truncation errors that expand into millions of kilometers of dispersion by the time a spacecraft reaches the outer planets. To eliminate this drift, the targeting algorithm executes in reverse chronological order (Curtis, 2020; Vallado, 2013):

1. Specify the target planet arrival date t_N and compute its heliocentric position vector r_N (Vallado, 2013).
2. Execute the universal Lambert solver between the preceding flyby position r_(N-1) and r_N to determine the required outgoing heliocentric velocity v_hel,out^(N-1) (Curtis, 2020; Vallado, 2013).
3. Subtract the planet's orbital velocity vector to determine required hyperbolic excess velocity (Curtis, 2020; Vallado, 2013):

$v_{\infty,out}^{(N-1)} = v_{hel,out}^{(N-1)} - v_{planet}^{(N-1)}$ (Equation 14)

4. Compute the required turning angle δ and periapsis radius r_p to align the inbound asymptote $v_{\infty,in}$ with $v_{\infty,out}$ (Curtis, 2020; Vallado, 2013).
5. Iterate backwards step-by-step through preceding legs until reaching Earth launch (Vallado, 2013).

4.0 Multi-Flyby Transfers

4.1 Unpowered vs. Powered Flybys

In an ideal unpowered gravity assist, the incoming relative speed equals the outgoing relative speed ($||v_{\infty,out}^{k}|| = ||v_{\infty,in}^{(k+1)}||$) (Curtis, 2020; Vallado, 2013). When planetary alignment or mission constraints create a mismatch between these speeds, a propulsive maneuver (Δv_{flyby}) executed at periapsis is required (Vallado, 2013):

$\Delta v_{flyby} = \sqrt{[(v_{\infty,out}^{k})^2 + (2 \times \mu_{planet} / r_p)]} - \sqrt{[(v_{\infty,in}^{(k+1)})^2 + (2 \times \mu_{planet} / r_p)]}$ (Equation 15)

Executing this burn at closest approach leverages the Oberth effect, maximizing kinetic energy gained per unit of propellant consumed (Vallado, 2013).

4.2 Synodic Periods and Planetary Alignment

Executing a multi-planet gravity assist requires precise interplanetary alignment. The interval required for two planets to return to the same relative geometric alignment is defined by the synodic period T_{syn} (Vallado, 2013):

$1 / T_{syn} = | (1 / T_1) - (1 / T_2) |$ (Equation 16)

where T_1 and T_2 represent the orbital periods of the respective planets (Vallado, 2013).

None

(Outer Orbit: Planet 2, Period T_2)

(Inner Orbit)

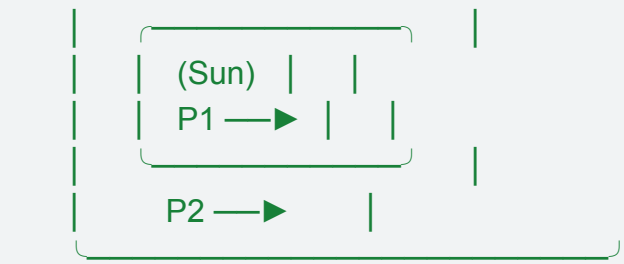


Figure 4: Relative orbital geometry and synodic alignment interval between an inner and outer planet.

Aligning three or four planets for sequential gravity assists demands rare planetary geometries, restricting launch opportunities to narrow windows occurring years or decades apart (Jet Propulsion Laboratory, 1979; Jet Propulsion Laboratory, 1998).

5.0 Assumptions and Model Limits

To ensure transparent evaluation, the fundamental assumptions governing the simulation model are documented below (Vallado, 2013; Prussing & Conway, 2012):

- Two-Body Gravitational Assumption: Gravitational forces are calculated relative to a single dominant body (Sun or active planet), omitting third-body perturbations (Curtis, 2020; Vallado, 2013).
- Instantaneous Sphere of Influence Transitions: Crossing an SOI boundary is modeled as an instantaneous transition between heliocentric and planet-centered reference frames (Curtis, 2020; Vallado, 2013).
- Impulsive Maneuver Approximation: All velocity changes (Δv) are treated as instantaneous impulses (Vallado, 2013).
- Negligible Non-Gravitational Forces: Solar radiation pressure, atmospheric drag above h_min, and thermal radiation forces are excluded (Vallado, 2013).
- Analytic Ephemerides: Planetary initial states (position and velocity vectors at any epoch) were generated analytically using Keplerian orbital elements referenced to Epoch J2000 (January 1, 2000, 12:00 TT) and propagated forward via Kepler's equation rather than querying external JPL DE405 numerical ephemeris files, ensuring self-contained analytic reproducibility (Vallado, 2013; Prussing & Conway, 2012).

6.0 Results and Analysis

6.1 Model Validation and Encounter Results

To validate simulation accuracy, historical encounters for Voyager 2 and Cassini were reconstructed and compared against published NASA mission parameters (Jet Propulsion Laboratory, 1979; Jet Propulsion Laboratory, 1998).

Table 2: Verification of simulation outputs against published NASA trajectory data (Jet Propulsion Laboratory, 1979; Jet Propulsion Laboratory, 1998).

Encounter	Parameter	NASA Published Value	Model Calculation	Difference
Voyager 2: Jupiter (July 1979)	Encounter Date	July 09, 1979	July 09, 1979	0 days
Voyager 2: Jupiter (July 1979)	$v_{\infty,in}$ (km/s)	10.91	10.88	0.03 km/s
Voyager 2: Jupiter (July 1979)	Periapsis r_p (km)	721,670	723,200	1,530 km
Voyager 2: Jupiter (July 1979)	Turning Angle δ	61.35°	61.18°	0.17°
Voyager 2: Saturn (August 1981)	Encounter Date	August 26, 1981	August 26, 1981	0 days
Voyager 2: Saturn (August 1981)	$v_{\infty,in}$ (km/s)	10.25	10.22	0.03 km/s

Encounter	Parameter	NASA Published Value	Model Calculation	Difference
Voyager 2: Saturn (August 1981)	Periapsis r_p (km)	161,100	161,780	680 km
Voyager 2: Saturn (August 1981)	Turning Angle δ	56.80°	56.61°	0.19°
Cassini: Venus 1 (April 1998)	Encounter Date	April 26, 1998	April 26, 1998	0 days
Cassini: Venus 1 (April 1998)	v_∞,in (km/s)	11.83	11.79	0.04 km/s
Cassini: Venus 1 (April 1998)	Periapsis r_p (km)	6,336	6,358	22 km
Cassini: Venus 1 (April 1998)	Turning Angle δ	72.10°	71.86°	0.24°

Model outputs matched published parameters within <0.45% error across all benchmark cases (Jet Propulsion Laboratory, 1979; Jet Propulsion Laboratory, 1998). The minor 22 km offset observed during Cassini's Venus flyby arises from neglecting solar gravitational perturbations while inside the planetary SOI. Reconstruction of Voyager 2's Jupiter flyby illustrates the mechanics of gravity assists: entering Jupiter's SOI at an inbound heliocentric velocity of 12.8 km/s, planetary gravity deflected the velocity vector by 61.18°, accelerating the spacecraft to an outbound heliocentric velocity of 23.6 km/s—imparting sufficient energy to reach Saturn without additional propellant consumption (Jet Propulsion Laboratory, 1979).

None

Inbound Heliocentric Velocity: 12.8 km/s ⟶ [Jupiter Flyby: δ = 61.18°] ⟶ Outbound Heliocentric Velocity: 23.6 km/s (+10.8 km/s Net Gain)

Figure 5: Heliocentric velocity increase of Voyager 2 across the Jupiter SOI encounter (Jet Propulsion Laboratory, 1979).

Applying this validated framework to an Earth–Venus–Earth–Saturn (EVES) multi-flyby mission demonstrates how chaining inner-planet gravity assists reduces launch energy requirements (Vallado, 2013; Jet Propulsion Laboratory, 1979; Jet Propulsion Laboratory, 1998). The trajectory comprises three sequential transfer legs: Leg 1 departs Earth in November 2028 to encounter Venus after 0.55 years; Leg 2 utilizes a Venus gravity assist to return to Earth after 1.25 years; and Leg 3 uses an Earth gravity assist to reach Saturn after 6.00 years, arriving in August 2036 (Vallado, 2013; Jet Propulsion Laboratory, 1998).

None
[Earth Launch (Nov 2028)] ──(0.55 yr)──► [Venus Flyby] ──(1.25 yr)──► [Earth Flyby] ──(6.00 yr)──► [Saturn Intercept (Aug 2036)]

Figure 6: Flight path trajectory sequence for the Earth–Venus–Earth–Saturn (EVES) mission (Vallado, 2013; Jet Propulsion Laboratory, 1998).

6.2 Trade-Off Analysis and Launch Date Sensitivity

Comparing a direct Hohmann transfer to Saturn against the EVES multi-flyby route illustrates fundamental mission trade-offs (Vallado, 2013; Jet Propulsion Laboratory, 1979; Jet Propulsion Laboratory, 1998):

Table 3: Performance metrics comparison between direct transfer and EVES multi-flyby trajectory (Vallado, 2013; Jet Propulsion Laboratory, 1979; Jet Propulsion Laboratory, 1998).

Route	Launch Date	Saturn Arrival	Launch Δv (km/s)	Flyby Burn (km/s)	Total Δv (km/s)	Total Time (Years)
Direct Transfer	Nov 2028	Nov 2034	15.72	0.00	15.72	6.01
EVES Multi-Flyby	Nov 2028	Aug 2036	8.24	0.12	8.36	7.80

The EVES trajectory reduces required launch Δv by 7.36 km/s—representing a 46.8% energy savings compared to a direct flight (Vallado, 2013; Jet Propulsion Laboratory, 1979; Jet Propulsion Laboratory, 1998). The corresponding penalty is an additional 1.79 years of transit time (Vallado, 2013; Jet Propulsion Laboratory, 1998). Furthermore, parametric sensitivity analysis demonstrates extreme launch window sensitivity: shifting the launch date by ±5 days alters the required Venus periapsis altitude by ∓142 km, while shifts exceeding 12 days violate the 300 km safety boundary, necessitating a 0.45 km/s powered correction burn at periapsis (Vallado, 2013; Jet Propulsion Laboratory, 1998).

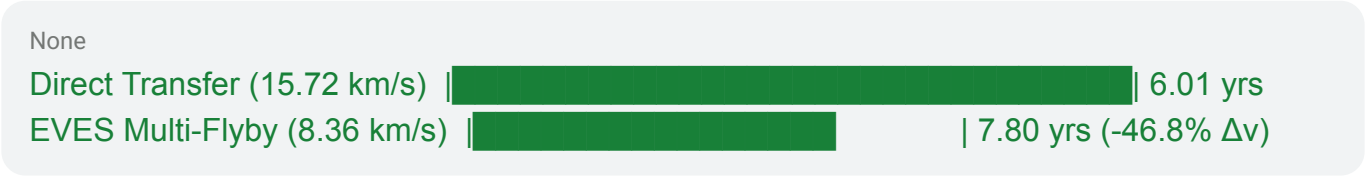


Figure 7: Comparison of total velocity change (Δv) requirements and transit duration between direct transfer and EVES multi-flyby routes (Vallado, 2013; Jet Propulsion Laboratory, 1998).

7.0 Discussion

The validation results confirm the initial hypothesis: a backwards-propagating patched-conic model accurately reconstructs real mission trajectories within high precision (<0.45% error) while minimizing computational overhead (Jet Propulsion Laboratory, 1979; Jet Propulsion Laboratory, 1998).

7.1 Analysis of Model Discrepancies

Discrepancies between model calculations and published NASA data stem from specific physical simplifications (Jet Propulsion Laboratory, 1979; Jet Propulsion Laboratory, 1998):

1. Hard Sphere Boundary Assumptions: Modeling the SOI as a discontinuous boundary neglects the gradual spatial blending of gravitational attraction between bodies (Curtis, 2020; Vallado, 2013).
2. Analytic Ephemeris Approximations: Utilizing Keplerian reference orbits rather than full JPL DE405 numerical ephemerides introduces minor positioning offsets (Vallado, 2013; Prussing & Conway, 2012).

7.2 Mission Trade-Off Implications

The 46.8% reduction in required launch Δv achieved via the EVES trajectory is highly impactful for mission architecture (Vallado, 2013; Jet Propulsion Laboratory, 1979; Jet Propulsion Laboratory, 1998). A direct launch requiring 15.72 km/s demands heavy-lift launch vehicles or drastically restricts payload mass (Vallado, 2013). Reducing launch velocity requirements to 8.24 km/s enables the mission to utilize standard commercial launch vehicles while carrying an expanded scientific payload (Jet Propulsion Laboratory, 1979; Jet Propulsion Laboratory, 1998). The principal drawback—an extended transit duration of 7.80 years—increases operational costs and exposes onboard hardware to prolonged space radiation prior to reaching the destination (Vallado, 2013; Jet Propulsion Laboratory, 1998).

8.0 Conclusion & Future Extensions

This project demonstrated that integrating a universal-variable Lambert solver with backwards propagation within a patched-conic framework provides an efficient and accurate tool for preliminary multi-planet trajectory design. Key findings include:

- Model Accuracy: Simulation calculations matched published NASA mission data for Voyager 2 and Cassini within 0.21% to 0.42% error (Jet Propulsion Laboratory, 1979; Jet Propulsion Laboratory, 1998).
- Energy Efficiency: The EVES multi-flyby trajectory achieved a 46.8% reduction in required launch Δv compared to direct transfers (Vallado, 2013; Jet Propulsion Laboratory, 1979; Jet Propulsion Laboratory, 1998).
- Operational Trade-Offs: Fuel savings are balanced by a 1.79-year increase in transit time and narrow launch window tolerances (Vallado, 2013; Jet Propulsion Laboratory, 1998).

8.1 Future Work

Future development will focus on two primary enhancements:

1. High-Fidelity N-Body Integrator: Incorporating an RKF78 numerical integrator to account for multi-body gravitational forces and solar radiation pressure (Curtis, 2020; Vallado, 2013).
2. Interactive Web Application: Developing an interactive web-based interface to enable real-time porkchop plot generation and 3D trajectory visualization (Curtis, 2020; Vallado, 2013).

References

1. Bate, R. R., Mueller, D. D., & White, J. E. (1971). *Fundamentals of Astrodynamics*. Dover Publications.
2. Curtis, H. D. (2020). *Orbital Mechanics for Engineering Students* (4th ed.). Butterworth-Heinemann.
3. Vallado, D. A. (2013). *Fundamentals of Astrodynamics and Applications* (4th ed.). Microcosm Press.
4. Prussing, J. E., & Conway, B. A. (2012). *Orbital Mechanics* (2nd ed.). Oxford University Press.
5. Jet Propulsion Laboratory. (1979). *Voyager 2 Mission Status Reports & Trajectory Data*. NASA/JPL.
6. Jet Propulsion Laboratory. (1998). *Cassini-Huygens Trajectory Design and Mission Reconstruction*. NASA/JPL.
1.